Organic Electronics 14 (2013) 2284–2289

Contents lists available at SciVerse ScienceDirect

Organic Electronics

journal homepage: www.elsevier.com/locate/orgel

A cascade energy band structure enhances the carrier energy in organic vertical-type triodes

Shiau-Shin Cheng [a], Mohan Ramesh [b,c], Guan-Yuan Chen [a], Chun-Lin Fung [a], Li-Ming Chen [a], Meng-Chyi Wu [a], Hong-Cheu Lin [b], Chih-Wei Chu [c,d,*]

[a] Department of Electrical Engineering, National Tsing-Hua University, Hsinchu 30013, Taiwan, ROC
[b] Department of Materials Science and Engineering, National Chiao Tung University, Hsinchu 30010, Taiwan, ROC
[c] Research Center for Applied Sciences, Academia Sinica, Taipei 11529, Taiwan, ROC
[d] Department of Photonics, National Chiao-Tung University, Hsinchu 30010, Taiwan, ROC

ARTICLE INFO

Article history:
Received 4 April 2013
Received in revised form 8 May 2013
Accepted 11 May 2013
Available online 4 June 2013

Keywords:
Organic semiconductor
Vertical-type transistor
Cascade-type
Transport factor
Current gain
Current mirror

ABSTRACT

Organic vertical-type triodes (OVTs) based on the cascade energy band structure as emitter layer are studied. The electric characteristics were dramatically enhanced while incorporating the cascade energy under current driving and voltage driving modes. The improvement is attributed to that injection carriers can obtain higher energy through a stepwise energy level. When the device has a layered structure of F_{16}CuPC (10 nm)/PTCDI (10 nm)/pentacene (100 nm) in emitter, it exhibits a common-base transport factor of 0.99 and a common-emitter current gain of 225 under current driving mode and exhibits a high current modulation-exceeding −520 μA for a low collector voltage of −5 V and a base voltage of −5 V and the current on/off ratio of 10^3 under voltage driving mode. Furthermore, we realized first organic current mirror that exhibited out/in current ratio of 0.75 and output resistance of 10^5 Ω by using the OVTs.

1. Introduction

The study of organic thin film transistors (OTFTs) has attracted much interest for their potential use in high-value, low-cost electronics, such as displays, sensors, radio frequency identifications, and e-papers [1–4]. Recently, organic semiconductors with mobilities comparable with that of amorphous silicon have been realized [5–8]; nevertheless, OTFTs possessing the typical metal–oxide–semiconductor field effect transistor structure exhibit low output currents and low frequencies of operation because of their high resistivities and low carrier mobilities, which restrict their practical applications. Although shortening the channel length can further improve the device performance, this approach requires that state-of-art lithographic techniques, which are not practical for fabricating low-cost flexible electronics, be performed prior to organic semiconductor growth; in addition, the contact resistance between the source/drain electrodes and the organic semiconductor will dominate the device performance [9,10]. To realize the incorporation of OTFTs in most proposed applications, it will be necessary to improve not only the electrical properties of the organic materials but also the device structures. Organic vertical-type transistors are a promising technological option for improving device performance [11–16] because their channel lengths can be controlled precisely by varying the thickness of the active layer.

In the early days of inorganic semiconductor development, bipolar-junction transistors (BJTs)—the most important inorganic vertical-type transistors—were formed using n–p–n or p–n–p double homojunctions [17]. Due to their larger minority-carrier diffusion and base resistance, the operation speeds of BJTs are limited by the transition

* Corresponding author at: Department of Photonics, National Chiao-Tung University, Hsinchu 30010, Taiwan (ROC). Tel.: +886 2 27898000x70; fax: +886 2 27826680.
E-mail address: gchu@gate.sinica.edu.tw (C.-W. Chu).

1566-1199/$ - see front matter © 2013 Published by Elsevier B.V.
http://dx.doi.org/10.1016/j.orgel.2013.05.018

time [18]. To overcome this obstacle, unipolar hot-carrier transistors (HCTs) were developed, featuring a thin metallic base sandwiched between two semiconductors to serve as an emitter and a collector. If the depletion region at the metal–semiconductor junction of a Schottky diode is thinner than the junction capacitance of a pn diode, it results the lower resistance. To further improve their performance, cascade energy band structures, formed by the different element concentration ratios, have been incorporated in HCTs. Such structures enhance the carrier energy in emitter–base (EB) diodes; therefore, the carriers can be inhibited from contributing to the recombination current at the base electrode and effectively approach the collector electrode to increase the output current. To control the element concentration ratio accurately, the devices must be grown using expensive fabrication processes (e.g., molecular beam epitaxy, metal organic chemical vapor deposition). In addition, the carrier transport mechanism in such devices is based on band-type conduction and the carriers are affected by the acoustic phonons. Therefore, it is difficult to operate these devices at room temperature [19,20]. In contrast, organic thin films can be fabricated using simple processing techniques. In their corresponding devices, carrier transport occurs through tunneling between the localized states caused by defects and/or disorder states, with a conduction theory associated with phonon-activated hopping. Therefore, organic vertical transistors are readily operated at room-temperature and can be applied in low cost, flexible electronics [21,15,22]. Due to lower carrier mobility of the materials and the shorter mean free path in the base layer, the most of the carriers are recombined at the base electrode. Which lead to a lower common-emitter current gain and lack the apparent saturation region. Several approaches have been developed to improve these drawbacks (e.g.,) by inserting a hole injection enhancement layer (LiF or Al_2O_3) at the emitter–base junction or using a metal-grid base electrode [23–25]. When inserting a hole injection layer the tunneling barrier are formed, as a result of the emitter current being dominated by the tunneling current, with exhibiting a saturation region and enhanced current gain.

In this paper, we describe organic vertical triodes (OVTs) incorporating a cascade-type energy band structure that operate at pronounced saturation with high gain. The most injection carriers can obtain higher energy through a stepwise energy level, more carriers can surmount the thin metal base electrode and diffuse into the collector layer. Therefore, this device exhibits a larger transport factor and a current gain when operated in the current-driving mode. On the other hand, the device displays a larger current on/off ratio and a smaller offset voltage when operated in the voltage-driving mode. The device exhibits a sufficiently large current gain; a current mirror operated at a greater out/in current ratio (I_{out}/I_{in}) and a greater output resistance (r_o) is achieved by integrating two p-channel OVTs with a load resistor.

2. Experimental

Prior to deposition, the glass substrates were cleaned sequentially with detergent, acetone, and isopropyl alcohol followed by treating in an ultraviolet (UV) ozone cleaner for 15 min. The gold (Au) (30 nm) layer was deposited on the glass substrate to serve as a collector electrode. The copper phthalocyanine (CuPC) (50 nm) layer (Luminescence Technology) was thermally deposited on the Au layer to smooth the surface morphology and then the pentacene (270 nm) layer (Luminescence Technology), serving as the collector of the p-channel triode, was thermally evaporated. The aluminum (Al) (10 nm) strip was thermally evaporated onto the pentacene layer to function as the base electrode. Next, a thin Al film (15 nm), operating as the base electrode, was deposited on the strip. To study the effects of the materials with different highest occupied molecular orbital (HOMO) energy levels on the device performance, different organic semiconductor layers were thermally evaporated onto the thin Al film as shown in Table 1. Finally, films of molybdenum(VI) oxide (MoO_3) (30 nm) and Al (30 nm) were deposited onto the emitter layers of the five OVTs mentioned above to function as emitter electrodes. This process was performed with patterning through a metal mask. All organic materials and metal electrodes were deposited in a thermal evaporation chamber at a base pressure of 10^{-6} torr. The active area of the device (0.04 cm^2) was defined by the intersection of the emitter and collector electrodes. The current–voltage (I–V) characteristics of the devices were measured using a Keithley 4200 semiconductor parameter analyzer. All of the electrical characteristics of these devices were measured in dark environments.

3. Results and discussion

Fig. 1a and b presents the device configuration and the energy diagram of the emitter–base diodes, respectively [26–29]. The device, fabricated from two Schottky diodes, comprises a collector–base diode as the bottom diode and an emitter–base diode as the top diode. To form the Schottky diode, the active layer was sandwiched between Au and Al. To reduce the leakage current and the energy barrier between the metal and the organics, a CuPC film was used as the buffer layer in the collector–base diodes and MoO_3 was inserted as the carrier injection layer in the emitter–base diodes [30–33]. Several organic semiconductors–pentacene, *N*,*N*′-bis(naphth-1-yl)-*N*,*N*′-bis(phenyl)-benzidine(NPB), *N*,*N*8-dioctyl-3,4,9,10-perylene tetracarboxylic diimide(PTCDI), and copper(II) 1,2,3,4,8,9,10,11,15,16,17,18,22,23,24,25-hexadecafluoro-29H,31H-phthalocyanine (F_{16}CuPC)—with different energy levels were employed to form the cascade-type structure in the emitter–base diodes. To investigate the influence of the cascade-type energy structure in the emitter–base diodes, we fabricated five different devices by incorporating the various materials in the emitter–base diodes as shown in Table 1. All five different devices configuration were fabricated and characterized with same material in the collector–base diodes ((Au (30 nm)/CuPC (50 nm)/pentacene (270 nm)/Al (30 nm)/thin Al layer (10 nm)). Fig. 2a and c displays the common-base (CB) electrical characteristics of devices A and E, respectively; Fig. 2b and d present the common-emitter (CE) electrical characteristics of devices

Table 1
Parameters of the OVTs featuring various active layers in the EB diodes.

Device	Layer 1	Layer 2	Layer 3	α[a]	β[b]	Offset voltage
A	Pentacene (100 nm)			0.0025	0.0056	−1.7 V
B	Pentacene (100 nm)	NPB (20 nm)		0.45	0.74	−1.7 V
C	Pentacene (100 nm)	PTCDI (20 nm)		0.85	3.69	−1.4 V
D	Pentacene (100 nm)	F_{16}CuPC (20 nm)		0.77	1.24	−1.5 V
E	Pentacene (100 nm)	PTCDI (10 nm)	F_{16}CuPC (10 nm)	0.99	20.83	−0.8 V

[a] Operated under the CB mode at values of V_{CB} and I_{EB} of −5 V and 100 μA, respectively.
[b] Operated under the CE mode at values of V_{CE} and I_{BE} of −7 V and −100 μA, respectively.

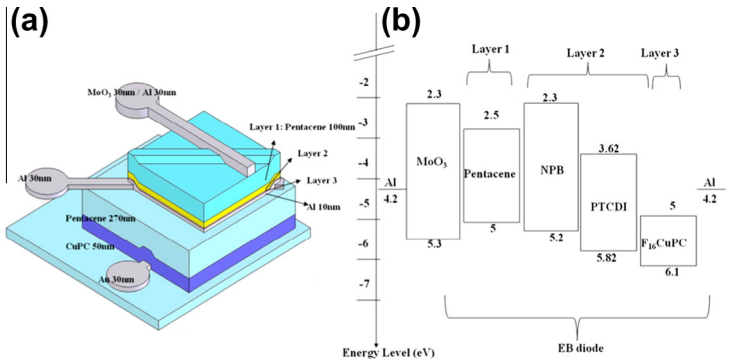

Fig. 1. (a) Schematic representation of the OVT configuration featuring a stepwise increase in the energy level, between the emitter electrode and base electrode, in the EB diode. (b) Energy level diagram of the organic semiconductors and metal in the EB diodes.

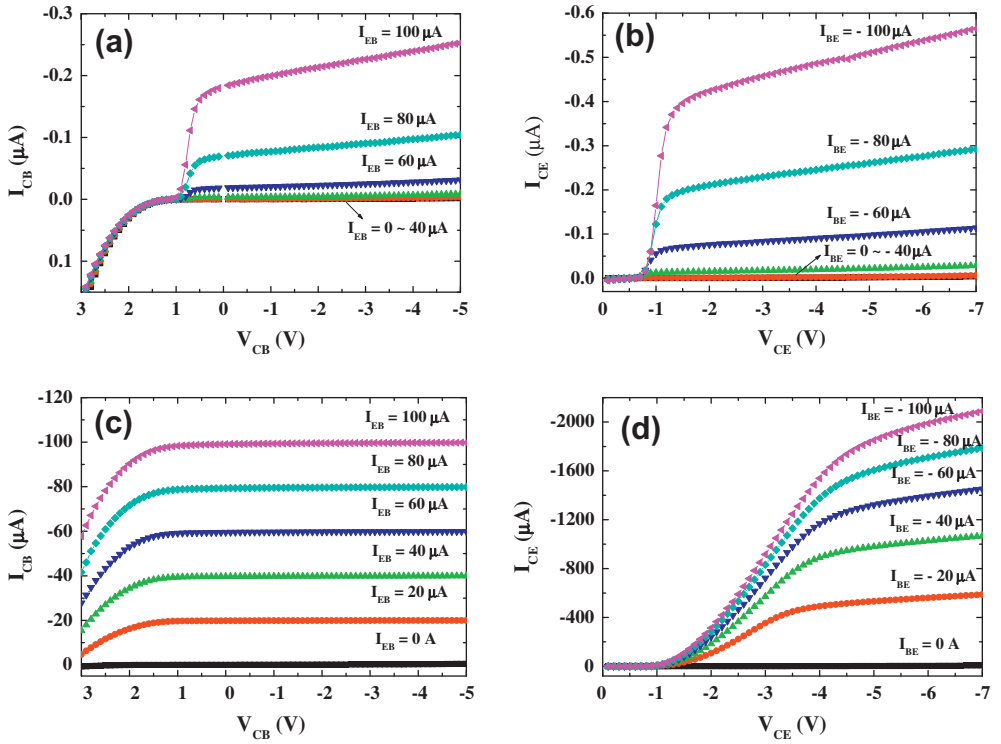

Fig. 2. (a and c) CB electrical characteristics of devices (a) A and (c) E for values of I_{EB} ranging from 0 to 100 μA with a step of 20 μA. (b and d) CE electrical characteristics of devices (b) A and (d) E for values of I_{BE} ranging from 0 to −100 μA with a step of −20 μA. The CB mode featured the base electrode grounded and the input current applied from the emitter electrode; the CE mode featured the emitter electrode grounded and the input current applied from the base electrode.

A and E, respectively. Both devices A and E could be operated with a pronounced saturation mode at low operating voltages. When devices A and E were operated under the CB mode at a collector-to-base current (I_{CB}) of 100 μA and a collector-to-base voltage (V_{CB}) of −5 V, the value of I_{CB} of device E (−99 μA) was larger than that (−0.25 μA) of device A; on the other hand, when devices A and E were operated under the CE mode at a base-to-emitter current (I_{BE}) of −100 μA and a collector-to-emitter voltage (V_{CE}) of −7 V, the collector-to-emitter current (I_{CE}) of device E (−2083 μA) was larger than that (−0.56 μA) of device A. The output current of device E was several orders of magnitude greater than that of device A in both the CB and CE modes. Presumably, the cascade energy structure of device E can create the higher energy carrier compare to device A. And it would also be easier to accelerate the carriers to achieve the ballistic velocity in the collector–base diode when it was operated under a low electrical field. In CB mode, the V_{CB} of device E was greater than 1 V, a positive collector current can be observed; which indicates that the carriers were ballistically transported into the collector and their velocity was almost constant, because the output current was independent of the applied electrical field. When the V_{CB} was less than 1 V would lead to the negative collector current. Which means that the carriers could not ballistically transported into the collector part, because the emitter current bend the energy band of the active layer in the collector–base diode. Therefore, the output current was proportional to the applied electrical field, when characteristics of the device were observed under the linear region (active region). The output current of the cascade energy structure operated under the saturation region at lower values of V_{CB}. In addition, carriers of higher energy could be transported into the collector layer efficiently to enhance the CB transport factor (α) and the CE current gain (β), which determine the device performance. The values of α and β, are given by the following the equations [17]:

$$\alpha = \frac{I_{CB} - I_{CB}(I_{E_B} = 0A)}{I_{EB}} \quad (1)$$

$$\beta = \frac{I_{CE} - I_{CE}(I_{B_E} = 0A)}{I_{B_E}} \quad (2)$$

Using Eqs. (1) and (2), the values of α for devices A and E were 0.0025 and 0.99, respectively, at a value of V_{CB} of −5 V and a value of I_{EB} of 100 μA; the values of β were 0.0056 and 20.83, respectively, at a value of V_{CE} of −7 V and a value of I_{BE} of −100 μA. Thus, the OVT incorporating the cascade energy structure exhibited significant enhancements in its values of both α and β. Table 1 summarizes the values of α and β of the OVTs incorporating the various emitter–base diodes.

The difference between the energy level of HOMO (F_{16}CuPC) and the work-function of the Al layer (2 eV) in device E, fewer holes become part of the recombination current at the base layer and most could pass through the base layer. Therefore, the CB transport factor α was close to unity and a larger CE current gain β was obtained. A larger carrier energy cannot only reduce carrier recombination at the base electrode but also increase the hopping rate. The probability of carriers hopping from the initial state to the next state is provided by the equation [34]

$$\gamma_{ij} = \gamma_0 f(E_i) \exp\left(-\frac{E_i - E_j}{kT}\right) \exp\left(-\frac{2R_{ij}}{a}\right) \quad (3)$$

where $f(E_i)$ is the Fermi function of the initial state, γ_0 is a constant related to the carrier–phonon coupling term, k is the Boltzmann constant, and T is the temperature; E_i and E_j are the energies of the initial state and the next state respectively and R_{ij} is the distance between them. In organic electronics, charge transfer across at the metal–organic semiconductor heterojunction. The redistribution of electron cloud and the interfacial chemical reactions result in an interface dipole forming immediately by increasing the barrier height between the metal and organic semiconductor [35,36]. Therefore, previous studies have found that the Schottky energy barrier exhibits the resultant energy barrier at the metal–organic semiconductor heterojunction, when the barrier height is greater than 0.4 eV [37,38]. In contrast, when an organic semiconductor is deposited on the organic thin film, the dipole forces would be weaker—or even negligible, because the organic semiconductor–organic semiconductor junction would feature weak intermolecular van der Waals forces [39,40]. Therefore, the energy level would be aligned with a flat energy at the interface junction and the carriers could be activated thermally by the electrical field to pass through the barrier into the next organic semiconductor layer. According to Eq. (3), a larger difference in energy between the initial state and the next state would lead to a higher hopping rate; nevertheless, a larger barrier between the two states would block the carrier transport. In device D, the energy barrier between pentacene and F_{16}CuPC is 1.2 eV and accordingly, the performance of this device was poorer than that of device C. Therefore, to further enhance the hole energy, we increased the HOMO energy levels of the materials in device E in a stepwise manner, resulting in this device exhibiting the highest performance. Presumably, the performance could be further improved by selecting a new material with a larger HOMO energy level to replace the F_{16}CuPC layer or through its insertion in the F_{16}CuPC/Al heterojunction.

Fig. 3 presents the values of α and β of device E as a function of the input current. The value of α varied from as low as 0.6 at an input current of 0.2 μA to as high as

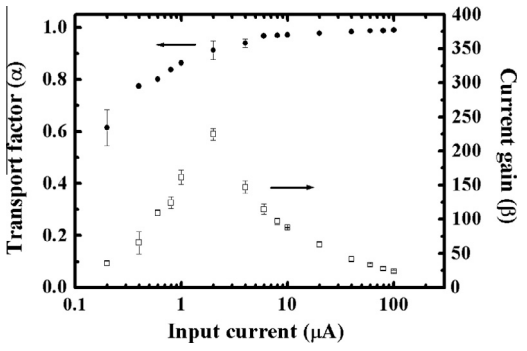

Fig. 3. Transport factor (α,●, left axis) and current gain (β, □, right axis) of device E, plotted as a function of the input current.

0.99 at an input current of 100 μA. The value of β also varied upon changing the input current by reaching a maximum value of 225 at an input current of 2 μA. When the device was operated at lower input currents, the induced input voltage was too low to turn on the emitter–base diode of the OVT and lower values of α and β were obtained. Increasing the input current would increase the induced input voltage, causing the emitter–base diode to be turned on. If the value of β too large an input current would cause space-charge effects in the emitter and collector, resulting in increased series resistance in these devices [41]. In our case, β reached its maximum value at an input current of 2 μA. To the best of our knowledge, this value of β is the highest ever reported for an organic vertical-type transistor [42,43].

The OVTs employ operation procedures similar to those of both BJTs and planar-type OTFTs. Fig. 4a and b presents the output characteristics of devices A and E, respectively. Between them, device E exhibited a lower offset and a much higher output current. The value of I_{CE} of the OVT reached as high as −521 μA with an offset voltage of −0.8 V when the base-to-emitter voltage (V_{BE}) and V_{CE} were both applied at −5 V. The current on/off ratio, defined as I_{CE} (V_{BE} = −5 V)/I_{CE} (V_{BE} = 0 V), was approximately 10^3 at a value of V_{CE} of −5 V. Because the value of I_{CE} is the sum of the output currents of the emitter–base and collector–base diodes, when the collector–base diode was operated at a low value of $|V_{CE}|$ under a forward bias, the leakage current observed was mainly attributed to the emitter–base diode. The positive current was proportional to V_{BE} at low values of V_{CE}. Upon increasing the value of V_{CE}, the value of I_{CE} transformed from a positive current into a negative current. The offset voltage is defined as the value of V_{CE} at which I_{CE} is equal to zero. At low values of V_{CE}, the leakage current was −3.16 nA and the offset voltage was −0.8 V. Decreasing the leakage current, which can be performed by increasing the value of α, would lead to a lowering of the offset voltage. Table 1 lists the offset voltages of devices featuring different active layers in the emitter–base diode.

Although the electrical applications of OVTs operated under the voltage-driving mode in integrated circuits have been realized [44], to the best of our knowledge, no academic or industrial research has been performed regarding the electrical applications of OVTs operated in the current-driving mode. A current mirror is an elemental cell in analog circuits, because it possesses lower input resistance and larger output resistance. Current mirrors have been fabricated using two or more transistors operated in the current-driving mode; they are designed to copy the current through one elemental cell by applying the input current into another elemental cell [45]. Therefore, the factors affecting the I_{out}/I_{in} ratio and the value of r_o (output resistance) play important roles in determining the performance of the current mirror. Having realized an OVT exhibiting a large value of β, we fabricated a current mirror by connecting the two OVTs with the base electrode in series and a resistor across the base and collector electrodes of a single OVT. Fig. 5a presents a schematic representation of the load-resistor current mirror incorporating the organic vertical-type triode; Fig. 5b displays I_{out} plotted with respect to I_{in} for devices with the various resistors at an output voltage (V_{out}) of −3 V. The resistor could support the bias voltage across the collector and base layer to drive the collector–base diode of the OVT. The larger resistor would drop the value of V_{in} in collector–base diode and the emitter–base diode could not be turned on; in addition, the smaller resistor would not drive the collector–base diode. Therefore, the largest I_{out}/I_{in} ratio, obtained when both OVTs were connected to a 100-Ω resistor, was approximately 0.75 and r_o (defined as V_{out}/I_{out} at a value of I_{in} of 0 A) was approximately 10^5. The input current can be defined using the equation

$$I_{in} = I_{CB} + \beta I_{BE} \quad (4)$$

when the current mirror is applied for input current, the OVT Q1 would induce the base voltage. Because the base electrode of OVT Q1 was connected to the base electrode of OVT Q2, the base voltage of Q2 was the same as that of Q1 and the output current was equal to the base current of Q2 multiplied by β. In the ideal case, the larger value of β and the smaller off current would result in an output current similar to the input current. We found that the OVT exhibited an off current that caused the output current to

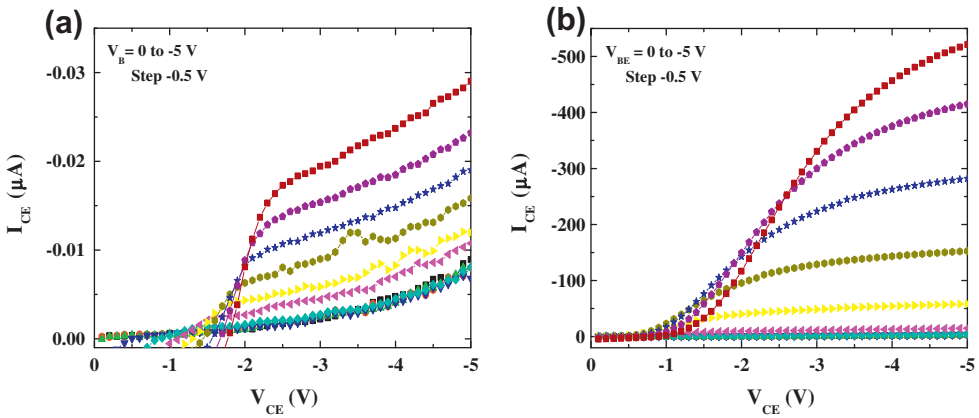

Fig. 4. Plots of I_{CE} versus V_{CE} for devices (a) A and (b) E for values of V_{BE} ranging from 0 to −5 V at a step of −0.5 V. The offset voltage (−0.8 V) for device E was less than that (−1.7 V) for device A.

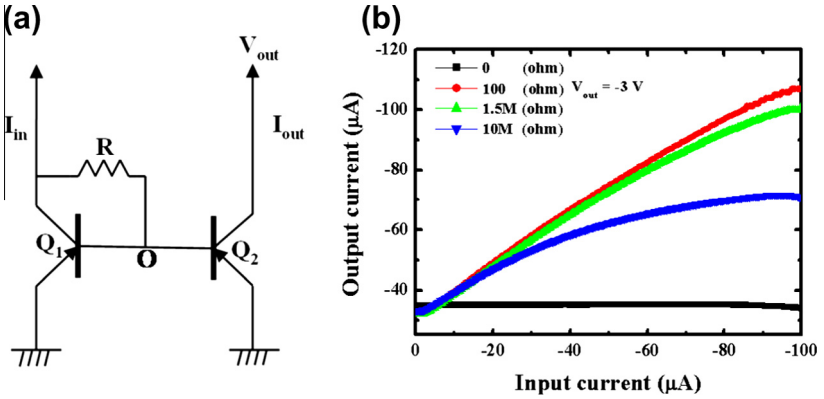

Fig. 5. (a) Schematic representation of the current mirror prepared from two OVTs (Q1, Q2) and a resistor (R). (b) Output currents of current mirrors connected with various resistances, plotted as a function of the input current. The output resistance and I_{out}/I_{in} ratio were $10^5\ \Omega$ and 0.75, respectively, when the values of R and V_{out} were 100 Ω and −3 V, respectively.

be different from the input current. Therefore, the I_{out}/I_{in} ratio and the value of r_o could be further improved by lowering the off current and/or increasing the value of β of the device.

4. Conclusion

In conclusion, we have realized a significant improvement in the electrical characteristics of OVTs by employing an appropriate cascade-type energy structure. Relatively high output currents and operation at low voltage were possible in both the current-driving and voltage-driving modes of the OVTs. We suspect that these properties might be improved further by optimizing the thickness of the organic layer or by choosing appropriate organic materials. Such high performance should increase the applicability of organic transistors.

Acknowledgments

We thank the National Science Council (NSC) of Taiwan (99-2221-E-001-012 and 99-2221-E-007-044-MY2) and Academia Sinica for financial support.

References

[1] D.J. Monsma, J.C. Lodder, T.J.A. Popma, B. Dieny, Phys. Rev. Lett. 74 (1995) 5260.
[2] C.D. Sheraw, L. Zhou, J.R. Huang, D.J. Gundlach, T.N. Jackson, Appl. Phys. Lett. 80 (2002) 1088.
[3] C.J. Drury, C.M.J. Mutsaers, C.M. Hart, M. Matters, D.M. de Leeuw, Appl. Phys. Lett. 73 (1998) 108.
[4] F. Eder, H. Klauk, M. Halik, U. Zschieschang, G. Schmid, C. Dehm, Appl. Phys. Lett. 84 (2004) 2673.
[5] Y.Y. Lin, D.J. Gundlach, S.F. Nelson, T.N. Jackson, IEEE Trans. Electron Dev. 44 (1997) 1325.
[6] A.A. Virkar, S. Mannsfeld, Z. Bao, N. Stingelin, Adv. Mater. 22 (2010) 3857.
[7] C.F. Sung, D. Kekuda, L.F. Chu, Y.Z. Lee, F.C. Chen, M.C. Wu, C.W. Chu, Adv. Mater. 21 (2009) 4845.
[8] C. Dimitrakopolous, R. Malenfant, Adv. Mater. 14 (2002) 99.
[9] D.J. Gundlach, L. Zhou, J.A. Nichols, T.N. Jackson, P.V. Necliudov, M.S. Shur, J. Appl. Phys. 100 (2006) 024509.
[10] A. Hoppe, J. Seekamp, T. Balster, G. Götz, P. Bäuerle, V. Wagner, Appl. Phys. Lett. 91 (2007) 132115.
[11] Y. Yang, A.J. Heeger, Nature 372 (1994) 344.
[12] L.P. Ma, Y. Yang, Appl. Phys. Lett. 85 (2004) 5084.
[13] M.S. Meruvia, I.A. Hümmelgen, Adv. Funct. Mater. 16 (2006) 459.
[14] K. Kudo, M. Iizuka, S. Kuniyoshi, K. Tanaka, Thin Solid Films 393 (2001) 362.
[15] Y.C. Chao, S.L. Yang, H.F. Meng, S.F. Horng, Appl. Phys. Lett. 87 (2005) 235508.
[16] T.M. Ou, S.S. Cheng, C.Y. Huang, M.C. Wu, I.M. Chan, S.Y. Lin, Y.J. Chan, Appl. Phys. Lett. 89 (2006) 183508.
[17] A.D. Neamen, Semiconductor Physics and Devices: Basic Principles, McGraw-Hill, Dubuque, 2003.
[18] A.F.J. Levi, T.H. Chiu, Appl. Phys. Lett. 51 (1987) 984.
[19] T.H. Chiu, W.T. Tsang, A.F.J. Levi, Electron. Lett. 17 (1987) 917.
[20] C.C. Wu, S.S. Lu, IEEE Electron. Dev. Lett. 13 (1992) 418.
[21] Z. Xu, S.H. Li, L. Ma, G. Li, Y. Yang, Appl. Phys. Lett. 91 (2007) 092911.
[22] K. Kudo, S. Tanaka, M. Iizuka, M. Nakamura, Thin Solid Films 438 (2003) 330.
[23] S.S. Cheng, C.Y. Yan, Y.C. Chuang, C.W. Ou, M.C. Wu, S.Y. Lin, Y.J. Chan, Appl. Phys. Lett. 90 (2007) 153509.
[24] Y.C. Chao, H.F. Meng, S.F. Horng, C.S. Hsu, Org. Electron. 9 (2008) 310.
[25] Y.C. Chao, M.H. Xie, M.Z. Dai, H.F. Meng, S.F. Horng, C.S. Hsu, Appl. Phys. Lett. 92 (2008) 093310.
[26] A.M.C. Ng, A.B. Djurisic, K.H. Tam, K.W. Cheng, W.K. Chan, H.L. Tam, K.W. Cheah, A.W. Lu, J. Chan, A.D. Rakic, Opt. Commun. 281 (2008) 2498.
[27] Y. Duan, M. Mazzeo, V. Maiorano, F. Mariano, D. Qin, R. Cingolani, G. Gigli, Appl. Phys. Lett. 92 (2007) 113304.
[28] H. Peisert, M. Knupfer, T. Schwieger, G.G. Fuentes, D. Olligs, J. Fink, T. Schmidt, J. Appl. Phys. 93 (2003) 9683.
[29] H.J. Bolink, E. Coronado, D. Repetto, M. Sessolo, E.M. Barea, J. Bisquert, G.G. Belmonte, J. Prochazka, L. Kavan, Adv. Funct. Mater. 18 (2008) 145.
[30] S.S. Cheng, Y.C. Chuang, D. Kekuda, C.W. Ou, M.C. Wu, C.W. Chu, Adv. Mater. 21 (2009) 1860.
[31] S.S. Cheng, J.H. Chen, G.Y. Chen, D. Kekuda, M.C. Wu, C.W. Chu, Org. Electron. 10 (2009) 1636.
[32] C.W. Chu, S.H. Li, C.W. Chen, V. Shrotriya, Y. Yang, Appl. Phys. Lett. 87 (2005) 193508.
[33] M. Yi, S. Yu, C. Feng, T. Zhang, D. Ma, M.S. Meruvia, I.A. Hummelgen, Org. Electron. 8 (2007) 311.
[34] A. Miller, E. Abrahams, Phys. Rev. 120 (1960) 745.
[35] N.J. Watkins, L. Yan, Y.L. Gao, Appl. Phys. Lett. 80 (2002) 4384.
[36] H. Ishii, K. Sugiyama, E. Ito, K. Seki, Adv. Mater. 11 (1990) 605.
[37] I.H. Campbell, D.L. Smith, Appl. Phys. Lett. 74 (1999) 561.
[38] A.K. Mahapatro, S. Ghosh, Appl. Phys. Lett. 74 (2002) 4840.
[39] J.X. Tang, C.S. Lee, S.T. Lee, J. Appl. Phys. 101 (2007) 064504.
[40] S. Kera, Y. Yabuuchi, H. Yamane, H. Setoyama, K.K. Okudaira, A. Kahn, N. Ueno, Phys. Rev. B 70 (2004) 085304.
[41] A.F.J. Levi, T.H. Chid, Phys. Scr. T23 (1988) 227.
[42] K. Nakayama, S. Fujimoto, M. Yokoyama, Appl. Phys. Lett. 88 (2006) 153512.
[43] C.Y. Yang, T.M. Ou, S.S. Cheng, M.C. Wu, S.Y. Lin, I.M. Chan, Y.J. Chan, Appl. Phys. Lett. 89 (2006) 183511.
[44] S.S. Cheng, G.Y. Chen, J.H. Chen, M.C. Wu, C.W. Chu, Org. Electron. 11 (2010) 692.
[45] A.S. Sedra, K.C. Smith, Microelectronic Circuits, Oxford University Press, New York, 1998.